DOI: 10.21062/mft.2024.066 http://www.journalmt.com

Mechanical Properties, Structure and Machinability of the H13 Tool Steel Produced by Material Extrusion

Martin Maly (0000-0002-9797-8632)[1,2], Stepan Kolomy (0000-0003-3781-692X)[1], Radek Kasan (0000-0002-5540-9335)[1,2], Lukas Bartl (0000-0002-8168-8462)[1,2], Josef Sedlak (0000-0002-9819-8259)[1], Jan Zouhar (0000-0001-8031-8366)[1]
[1]Institute of Manufacturing Technology, Faculty of Mechanical Engineering, Brno University of Technology, Technická 2896/2, 616 69 Brno, Czech Republic, E-mail: maly@vutbr.cz
[2]Central European Institute of Technology (CEITEC), Brno University of Technology, Purkyňova 656/123, 612 00 Brno, Czech Republic, E-mail: maly@vutbr.cz

The study focuses on an evaluation of mechanical properties of the H13 tool steel manufactured by the material extrusion and further comparison with conventionally produced material. Notably, for achieving sufficient surface quality of functional parts further post-processing is required. Thus, a comprehensive investigation, encompassing hardness, ultimate tensile strength (UTS) and yield strength (YS) measurement, microstructure, and machinability was performed. The material extrusion, an increasingly utilized additive manufacturing (AM) technique, offers a viable alternative to the prevalent laser powder bed fusion (LPBF) methods. The investigation revealed that the horizontal orientation of parts yielded the highest mechanical properties, reaching the ultimate tensile strength of approximately 1200 MPa. Additionally, the material exhibited the hardness of 47 HRC in the as-built state. The conventionally produced steel resulted in the higher UTS and YS in comparison to the AM material. The machinability of the as-built material in regard to cutting forces and surface roughness was also evaluated Lower surface roughness was achieved by decreasing feed per tooth. Optically measure material porosity was 6.13 % with maximum pore size 7.43 µm. The primary objective of this research is to optimize the mechanical properties of H13 tool steel post-printing, with a broader aim to apply the gained insights to improve other materials produced by the material extrusion.

Keywords: Material Extrusion, H13 Tool Steel, Additive Manufacturing, Microstructure, Mechanical Properties

1 Introduction

H-series steels are frequently employed in the production of dies, possessing characteristics that can withstand elevated loads and temperatures associated with forging processes. The H13 tool steel (1.2344, X40CrMoV5-1), a versatile and widely used material, excels in hot forging applications due to its unique combination of properties. The tempered H13 tool steel, achieved through double or triple tempering, features a remarkable set of characteristics, including high hardness, high UTS, excellent fracture toughness, and maximum fatigue strength at both room and elevated temperatures. The exceptional combination of properties is attributed to a presence of key alloying elements. The elevated amount of chromium enhances a resistance to high temperatures and oxidation, while molybdenum increases a hardenability. [1] The presence of vanadium contributes to a higher strength, improved toughness, and enhances fabrication and service performance. [1-3]

An alternative method of the production functional parts is commonly known as AM. This very often used method for fabrication of metal production parts is usually associated with LPBF [4]. This technique has been widely studied with association of H13 tool steel production [3,5-9]. Yonehara et al. [10] studied optimisation of the LPBF process. Density and microstructure of parts was evaluated including an influence of a laser power source. Produced parts achieved density of 99.9% when using the 400 W laser source. They also reduced the processing time by 30 % with the 1000 W laser source. Residual stresses of LPBFed parts were investigated by Narvan et al. [11]. They found out that residual stresses in high density parts (more than 97%) are independent on a densification level. Preheating of the part eliminates cracks but also stress-relief post-process is necessitated. Abdel-latif et al. [12] studied the mechanical properties and microstructure of LPBF tool steel. They proved that increasing scanning speed deteriorated the strength, ductility, impact toughness and hardness. The preheating effect on microstructure and mechanical properties was studied by Mertens et al. [7]. It was proved that higher preheating temperatures lead to stronger and more uniformal (homogenous microstructure) material and better mechanical properties then the part with no or

lower bed preheating but lead to generation tensile residual stresses.

Although powder bed fusion [13-14] is the most enhanced AM technology, material extrusion seems to be the alternative method with a great potential to be used in specific applications. Bose et al. [15] describe in their review also other additive manufacturing techniques. Timko et al. [16] compared material extrusion method and SLM. Besides others, it is shown that material extrusion method is more than two times cheaper than SLM. The material extrusion process involves 2 separate stages. The first stage is a layer by layer printing similar as in FDM process. Some of the key parameters, which influence final mechanical properties of the part, are number of perimeters, printing temperature, bed temperature, printing line strategy, infill pattern, layer thickness etc. A build sheet is usually used between part and build platform. The printed body is called a green body and must be further processed. The processing includes debinding and sintering which could be done in one or two stages. The debinding process washes out a polymer from the part and a brown body is created. During the sintering process, particles are sintered together and form the final solid part. Removing the binder from the input material during the second stage is a critical part of the material extrusion process due to cracks which could occurred in the part. The sintering is performed under a protective atmosphere to prevent the part from oxidation. The sintering stage plays a significant role in final mechanical properties of the produced part. Jansa et al. [17] studied mechanical properties of steel produced by material extrusion. It is known than mechanical properties of parts produced by material extrusion are typically lower compared to conventionally production methods. This could be caused by internal porous defects. Czan et al. [18] compared the working accuracy of material extrusion with SLM. The accuracy is strongly influenced by the manufacturing parameters and depends on geometry, orientation and position of the individual shape specifications of the 3D object. Degree accuracy of approximately IT12 to I13 was achieved.

Generally, the H13 tool steel is used for wear-resistant components, especially in injection molds and die-casting dies, due to its high toughness and heat resistance. Despite an excellent thermal shock resistance and a thermal fatigue resistance, H13 tool steel exhibits also some limitations in terms of a corrosion resistance and potential brittleness at elevated temperatures. Combining AM technique with the H13 tool steel production emerges new possibilities. The fabrication of injection molds with internal cooling channels could be one of them. These molds must exhibit excellent mechanical properties including surface quality. To achieve a desired surface quality, further post processing is necessary [19-21]. Mclean at al. [22] studied the effect of heat treatment and hot isostatic pressing on porosity which helps to improve the mechanical properties of additive manufactured parts. Gohn et al. [23] studied mold inserts for injection molding prototype applications fabricated by material extrusion. They proved that tooling prototyping can lower material costs for tooling validation and reduce engineering and equipment time. Papageorgiou et al. [24] investigated the usage of H13 as working die in plastic injection molding. It was shown that improper cooling condition can lead to fatigue corrosion cracking which further leads to damage of the die before predicted service life. Kuo et al. [25] describe in their study the importance of designed cooling channels. Different strategies of cooling channels were investigated, and conclusion was made.

Material extrusion seem to be the promising technology with the great potential and undisputed advantages to replace the traditional molds production method. Due to the limited number of studies regarding material extrusion of the H13 tool steel and its mechanical properties, the study was created. It describes the mechanical properties (tensile testing, compression tests) as well as evaluates material density, structure and machinability of H13 tool steel. The paper provides a good overview and helps to promote material extrusion method as a possible substitution of powder bed fusion technologies.

2 Materials and methods

2.1 Materials

The H13 tool steel from Desktop Metal has been used for this study. It is a composite rod containing of metal powder enclosed in a polymer binder and paraffin. The composition of the metal powder is shown in Tab. *1*. A safety risk combined with handling very fine metal powder is reduced by immobilizing the powder particles in the matrix of the filament binder. When comparing to the powder bed fusion technology (e.g. SLM, EBM.), handling of the material is much safer and does not require any specialized protective equipment [26]. 15 mm length rods with 1.5 mm in a diameter are stored in a container of 192 pieces with a mass of 4.2 kg. There are three main options how to extrude the material. Desktop Metal in Studio System uses a piston to extrude rods from the printer cartridge.

Tab. 1 *Chemical composition of the H13 tool steel powder*

Elements	Cr	Mo	Si	V	C	Mn	P	S	Fe
Reference Wt. %	4.8–5.5	1.1–1.7	0.8–1.2	0.8–1.2	0.3–0.45	0.2–0.6	Max. 0.03	Max. 0.03	Balance

2.2 Preparation of samples

The sample fabrication was performed on a Studio System (company Desktop Metal) 3D desktop printer using material extrusion technology under process parameters shown in Tab. 2. The conversion of dimensions after shrinkage was calculated in SW Fabricate (from Desktop Metal) according to manufacturer recommendations. The same software was used for slicing and for operating with Desktop Metal devices.

Tab. 2 *Printing process parameters used for material fabrication*

Nozzle diameter [mm]	Layer height [mm]	Infill type [-]	Nozzle temperature [°C]
0.4	0.1	Alternating lines	175
Bed temperature [°C]	**Print speed [mm.s^{-1}]**	**Chamber temperature control [°C]**	
65	15	YES, 50	

All of the printed samples were fabricated with a nozzle with 400 μm in diameter. All samples were printed with 100% density of a infill using an alternating line pattern shown in Fig. 1. The layer thickness used for the fabrication was set to 0.1 mm.

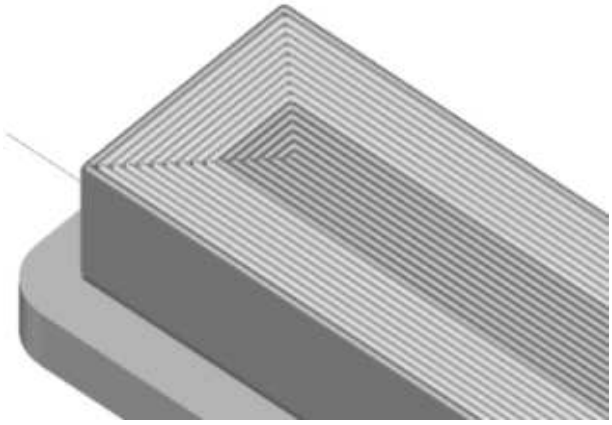

Fig. 1 *Printing strategy - alternating lines*

The debinding and sintering processes (all samples were debinded and sintered in one batch) were carried out in devices from Desktop Metal as a part of Studio System. A standard thermo-chemical procedure of the catalic debinding was used when green parts were heated to 44 °C. The duration of removing the binder varied according to the wall thickness of the sample. The porous brown parts were further sintered under pure argon atmosphere at the pressure and temperature bellow the material´s melting point. After the sintering stage, some of the samples were further post-processed. The samples for tensile tests were achieved by machining, which took place in a universal lathe (DMG CLX 350) and 5 axis milling machine (DMG DMU 50).

2.3 Mechanical properties tests

The tensile tests were performed according to ISO 6892 [27] on ZD40 tensile testing machine, which is suitable for tensile, compressive testing and is equipped with a force sensor. Three groups of samples were created for this type of testing. The samples in a group A were built in a vertical direction with a machining allowance within the full length. Samples in the groups B and C were 3D printed in the horizontal direction. The Group B had the machining allowance in full length and samples in group C had machining allowance only at the places where threads (used for sample clamping) were created by the machining. The machining process could influence mechanical properties of the samples. The upper layer could be inconsistent and the protrusions could consist of very hard grains.

2.4 Porosity measurement

There are several methods for measuring porosity [28]. The porosity in detail sample areas was evaluated by the software ImageJ and porosity in the whole sample cross section was performed by the optical microscope Olympus DSX 500 (used plugin for porosity evaluation). Observed cross-sections were conducted in horizontal and vertical directions. Measurements were performed under a 140 magnification. The whole observed area was than composed of many pictures in aims to cover the whole sample cross-section.

2.5 Microstructure observation

The microscopic observations involved the preparation of samples. The preparation process included cutting each sample using a LECO MSX metallographic cut-off saw and pressing it into a puck. Subsequently, the samples were ground and polished, with polishing performed using 1 μm and 0.5 μm diamond pastes. After polishing, the samples underwent etching with a 2% nital solution. The prepared samples were then subjected to a microscopic analysis. The optical microscopy was employed, utilizing an Olympus DSX500 microscope.

2.6 Machinability

Machinability testing was conducted using 3 mm diameter carbide solid end mill with TiN coating. Parameters which affect machinability are mainly cutting parameters, heat treatment, tool clamping, coolant, and workpiece material. The tool wear was evaluated at the end of each test under the optical microscope Olympus DSX 500.

The main aim was to evaluate the impact of cutting conditions (cutting speed (v_c) and feed per tooth (f_z)). All the tests were performed under dry machining conditions. The tool wear and surface roughness were evaluated. Cutting conditions of the experiment are shown in Tab. 3.

Tab. 3 *Cutting conditions used for machinability testing.*

Condition/test number	1.	2.	3.	4.	5.	6.
Cutting speed v_c [m.min^{-1}]	120	140	160	120	140	160
Feed rate f_z [mm]	0.0025	0.01	0.0175	0.0175	0.01	0.0025

3 Results and discussion

3.1 Samples characterization

In terms of verifying the composition of incoming materials in rods, the SEM analysis was done. It was proved that the chemical composition corresponds to the Tab. 1. The structure of the material is shown in Fig. 2. As can be seen, the structure consists of particles of different size. The maximum size of particles is 15 μm. The difference in particle dimension allows the favourable sintering process. The black spots in Fig. 2 are the polymer and wax.

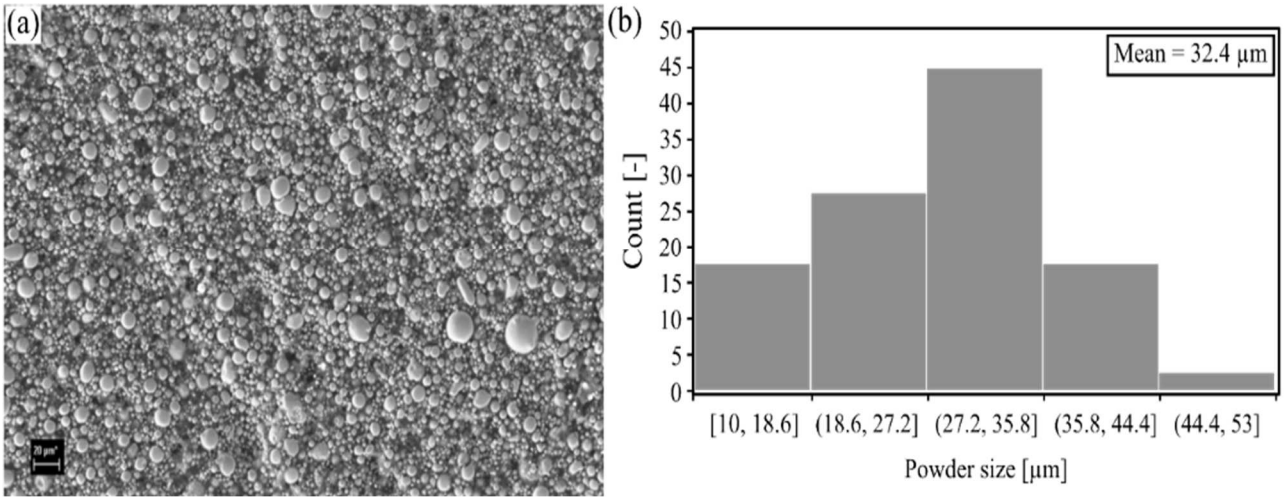

Fig. 2 *(a) Input rod SEM analysis structure, (b) Particle size distribution*

3.2 Mechanical and general properties evaluation

Three groups of additively manufactured samples were tested and compared to referenced material produced conventionally by a rolling. The description of samples can be seen in the Tab. 4.

Fig. 3 and Fig. 4 show obtained results from tensile testing of different types of samples listed in Tab. 4. YS, UTS and ductility (A Lo1) of 3D printed samples together with the reference material were evaluated. In comparison to reference samples, additively manufactured samples featured higher mechanical properties caused by the heat treatment during the sintering stage. Regarding YS, the vertically printed samples did not feature any plastic deformation. As seen in the Fig. 5c), there was brittle fracture on vertically printed samples after the tensile test. The fracture was created among deposited layers. In comparison with vertically printed sample, (in the Fig. 5b) there is the horizontally 3D printed sample after tensile test. There are visible holes among individual layers. The delamination of layers is visible in the pictures of horizontally printed samples. The fracture on the printed samples always starts on pores among individual layers. UTS and YS achieved similar values as far as the horizontally 3D printed samples is concerned. Fig. 5d shows the horizontally 3D printed samples without the allowance for machining. The as-printed layer is seen in the picture. It seems that this machined and unmachined surface featured no effect on mechanical properties of H13 tool steel created by the material extrusion. When comparing referenced sample and printed samples, printed samples featured only about 2 % ductility. Bechny et al. [29] described influence of part orientation in building chamber created by Binder Jetting on mechanical properties. The study shows that the orientation has minimum influence on final mechanical properties of printed part. This conclusion is different from results which were achieved in current study as shown in Fig. 3 and Fig 4. Novak et al. [30] proved strain at break 4.5 ± 0.3 % in samples from 17-4PH steel created by material extrusion.

Tab. 4 *Tensile test of vertically and horizontally printed samples*

Groups description of the samples	Label
Referenced as-rolled material	A
Horizontally as-built with the allowance for machining	B
Vertically as-built	C
Horizontally as-built without the allowance for machining	D

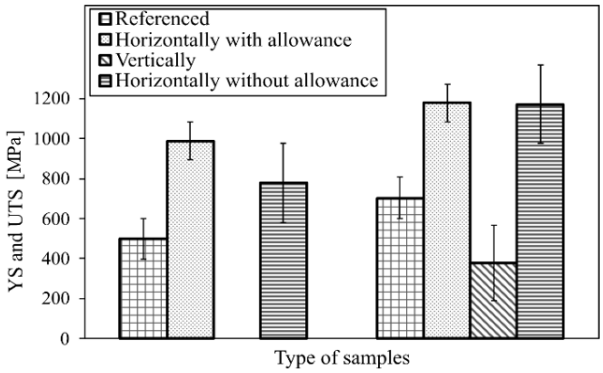

Fig. 3 *Mechanical properties established by tensile testing (yield strength and ultimate tensile strength)*

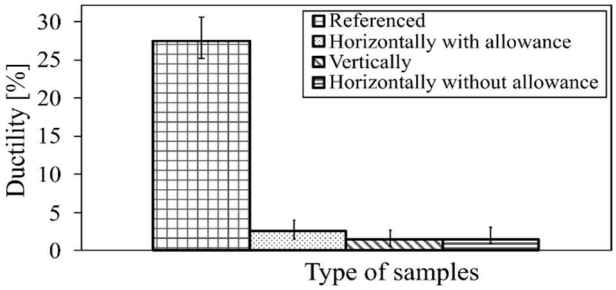

Fig. 4 *Ductility established by tensile testing*

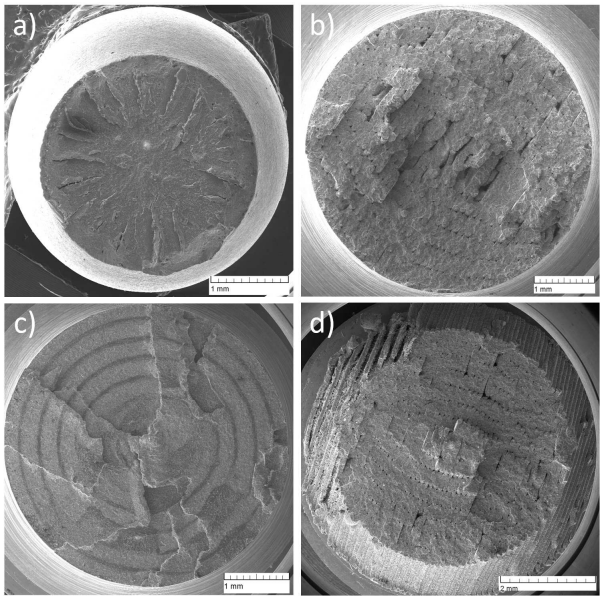

Fig. 5 *SEM images of the fracture surface for the different types of samples in group A (a), B (b), C (c), and D (d) after tensile test*

3.3 Porosity evaluation

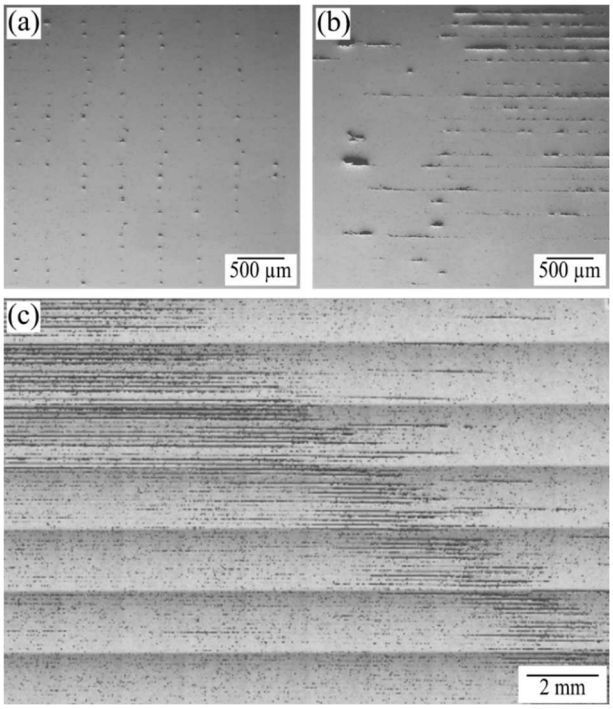

Fig. 6 *Porosity evaluation, (a) microporosity depicted in a perpendicular cross section, (b) microporosity depicted in a longitudinal cross section and (c) overall porosity evaluated in perpendicular cross section*

The porosity of individual 3D printed samples made of H13 tool steel was measured on as-built samples in horizontal and vertical cross sections. The cross section shown in Fig. 6a was performed in the horizontal direction and Fig. 6b depicts the vertical direction. The samples featured a 0.41 % and 2.09 % in the horizontal and vertical directions, respectively. As visible, there are holes among each deposited layer. This could be caused by not sufficient amount of extruded material during the sample fabrication, too much binder in the bulk material or low energy input during the sintering process. During the sintering process, powder particles need energy (time and temperature) to sinter together and close the gaps. Fig. 6c portrays the porosity evaluation in the whole sample cross section, which exhibited a 6.13 % with maximum pore size 7.434 µm. It can be seen that the pores occurred in the position corresponding to an individual layer deposition causing not a proper binding.

In other words, the pores within the sample structure were responsible for the brittle fracture of the vertically printed samples (described in section 3.3). Studies of Åsberg et al. [31] and Fryzowicz et al. [32] showed lower porosity when using different additive manufacturing techniques.

3.4 Structure characteristics

The Fig. 7 shows the microstructure of horizontally 3D printed samples. There are visible lines among each grain corresponding to prior austenite grains. The sintering process influenced the final structure by martensitic transformation. This could cause higher hardness resulting to the lower machinability. There are visible black spots (see Fig. 7b), which can be attributed to gaps such as pores and voids between extruded material. For reaching higher mechanical properties it is suitable to reduce these pores. Their existence can cause a possibility of a stress concentration, which reduces mechanical properties (as presented in chapter 3.2). Further post processing of as-built samples could lead to mechanical properties improvement.

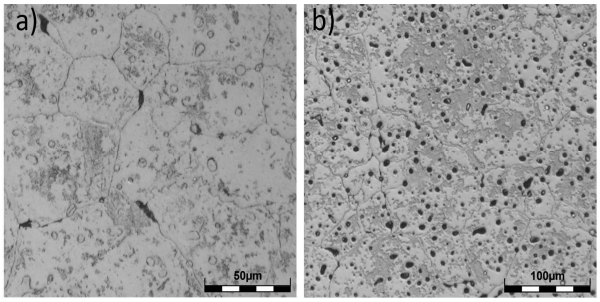

Fig. 7 *Structure of H13 tool steel a) lower magnification, b) higher magnification*

3.5 Machinability evaluation

The tool wear (TW) was evaluated via optical microscope Olympus DSX 500. Fig. 8 shows the milling tool after the machining test. There is TW depicted on clearance face (see Fig. 8a) and rake face (see Fig. 8b). Fig. 8c shows TW reached in tests 1-6. The point on the graph represents the average obtained TW calculated from the four measured cutting flutes. Additionally, the deviation, which corresponds to the highest and lowest measured TW values, is depicted. The lowest values of TW were achieved during the lowest cutting speed and feed per tooth. On the other hand, the highest TW were achieved during higher cutting speed and feed per tooth. Considering tests carried out with the same cutting speed, the higher TW was obtained in case of tests performed with higher feed per tooth (the similar results were observed by Liu et al. [33]). It can be seen that the clearance TW reached the lower value in comparison to the rake TW in all cutting tests. The highest obtained TW (0.33 mm and 0.35 mm for clearance TW and rake TW, respectively) was obtained in test 3 (the highest cutting conditions). On the other hand, the lowest TW (0.19 and 0.22 mm for clearance TW and rake TW, respectively) was observed under the lowest cutting conditions (see test 1). Obtained TW featured regular characteristics when dry machining of H13 tool steel. Further analysis of the material machinability under flood cooling would be our next topic. We have to take into account that flood cooling will probably reduce the tool life due to the cyclic change of tool temperature but decrease the surface roughness [34].

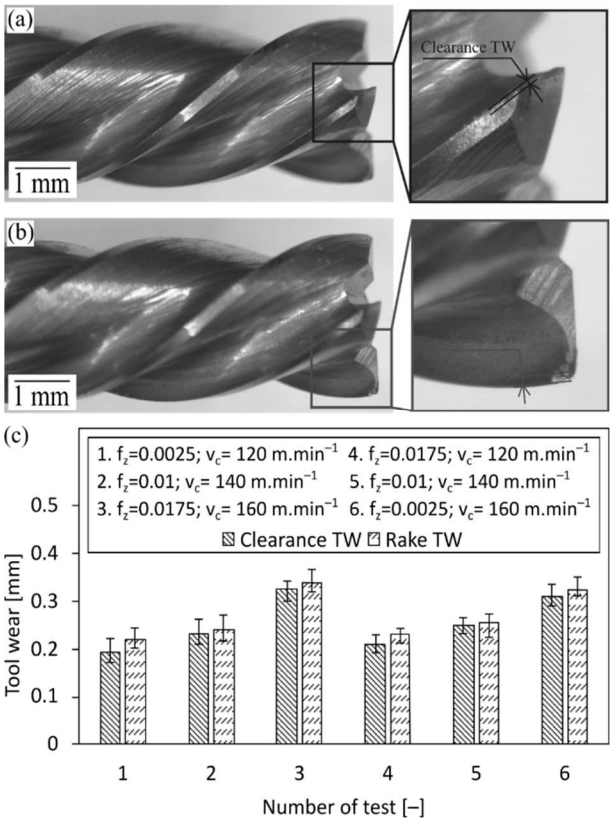

Fig. 8 *Images of tool wear obtained by the optical microscope at the end of the cutting test, (a) tool wear measured on clearance face, (b) tool wear measured on rake face and (c) visualization of tool wear for different cutting tests*

Regarding the surface roughness, results indicate a direct correlation between feed per tooth and surface roughness, such that increasing feed per tooth results to the higher surface roughness [35]. Cutting speed seems to have minimal influence on surface roughness as observed in [36]. The course of surface roughness increases with the increasing cutting length, which corresponds to the tool wear propagation. The test 3 exhibited the steepest increase in the surface roughness measurement corresponding to the highest cutting conditions, under which the highest TW was observed. Test 1 and 6 featured a very similar surface roughness due to the same feed per tooth. Globally, it can be concluded that the feed per tooth exhibited the

biggest influence on the final surface roughness (see test 2 and 5 performed under the highest feed per tooth), while cutting speed did not significantly affect the surface roughness. Similar results were obtained in [37].

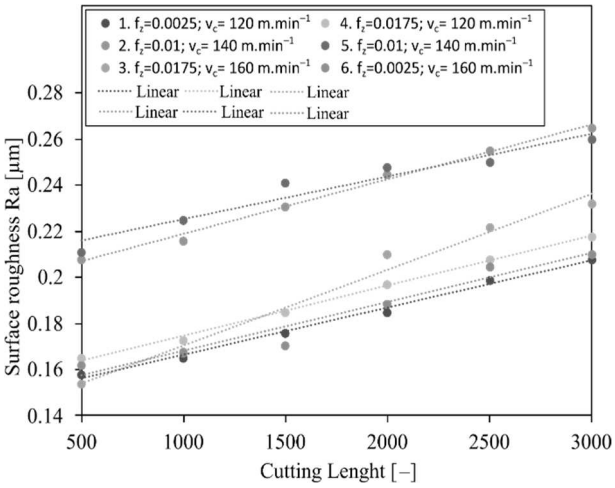

Fig. 9 *Surface roughness measurement in dependence on cutting length for each test 1-6*

Based on the obtained results it can be stated that the material extrusion method can be used for parts production. On the other hand, the as-built samples consisted of numerous pores uniformly distributed within the material structure. It was found that the pores are responsible for the lower mechanical properties. For reducing the final porosity and enhancing mechanical properties, a hot isostatic pressing (HIP) could be used. This investigation is going to be our next plan. It is important to note that the material machinability needs further investigation, because the machinability can differ in comparison to the conventional material. Hence our next plan is the machinability comparison between 3D printed and conventional materials.

4 Conclusion

Our research has demonstrated the feasibility of using the metal extrusion method to reliable printing of the H13 tool steel samples. Samples were manufactured in both horizontal and vertical orientations. These samples were used to characterize the mechanical properties of the processed H13 tool steel and were compared with conventionally produced material. Furthermore, the machining of the as-built H13 tool steel was performed under different cutting conditions to evaluate tool wear and surface roughness The key findings are summarized as follows:

- Powder particles were uniformly distributed in the binder, consistent with the typical composition of H13 tool steel.
- The printing strategy plays a significant role in influencing mechanical properties and final porosity.
- Vertically printed samples exhibited brittle fracture during tensile testing and exhibited significantly lower UTS compared to horizontally printed samples. The UTS of the horizontally 3D printed samples reached approx. 1200 MPa.
- The microstructure of 3D printed samples revealed numerous pores, primarily attributed to insufficient extrusion of metal material during the printing process. Upon binder removal, these pores formed gaps that could not be fully closed by following sintering process.
- Porosity was measured using optical microscope and featured a 0.41 % and 2.09 % in the horizontal and vertical directions, respectively the overall porosity exhibited a 6.13 % with the maximum pore size 7.434 μm within the horizontal cross section.
- The highest obtained tool wear (0.33 mm and 0.35 mm for clearance TW and rake TW, respectively) was obtained under the highest cutting conditions. On the other hand, the lowest cutting conditions resulted in the lowest TW (0.19 and 0.22 mm for clearance TW and rake TW, respectively).
- Globally, it can be concluded that the feed per tooth exhibited the biggest influence on the final surface roughness, while cutting speed did not significantly affect the surface roughness.

It is very hard to specify the optimal cutting conditions when machining of as-built H13, but based on the obtained resulted, to reach the lower surface roughness the lower feed per tooth is recommended. While various methods can enhance the mechanical properties of printed parts, the material extrusion will always exhibit different properties compared to conventionally manufactured parts. Further investigation is required to determine if the properties of material extrusion-printed parts are sufficient for specific applications. Future studies should focus on reducing porosity through HIP and improving the mechanical properties of 3D printed components. Nonetheless, material extrusion demonstrates promise as a technology for creating lightweight structures and parts with customized infill patterns.

Acknowledgement

This research study was supported by the grant "Modern technologies for processing advanced materials used for interdisciplinary applications", FSI-S-22-7957. This work has been performed in the project RICAIP: Research and Innovation Centre on Advanced Industrial Production which has received funding from the European Union's Horizon 2020 research and innovation program under grant agreement No 857306 and from the Ministry of Education, Youth and Sports under OP RDE grant agreement No CZ.02.1.01/0.0/0.0/17_043/0010085.

References

[1] NIE, Z., WANG, G., MCGUFFIN-CAWLEY, J.D., NARAYANAN, B., ZHANG, S., et al. (2016). Experimental study and modeling of H13 steel deposition using laser hot-wire additive manufacturing. In: *Journal of Materials Processing Technology*. Vol. 235, pp. 171-186. ISSN 09240136. https://doi.org/10.1016/j.jmatprotec.2016.04.006.

[2] FAYAZFAR, H., SALARIAN, M., ROGALSKY, A., SARKER, D., RUSSO, P., et al. (2018). A critical review of powder-based additive manufacturing of ferrous alloys: Process parameters, microstructure and mechanical properties. Vol. 144, pp. 98-128. ISSN 02641275. https://doi.org/10.1016/j.matdes.2018.02.018.

[3] COTTAM, R., WANG, J., LUZIN, V. (2014). Characterization of microstructure and residual stress in a 3D H13 tool steel component produced by additive manufacturing. In: *Journal of Materials Research*. Vol. 29, no. 17, pp. 1978-1986. ISSN 0884-2914. https://doi.org/10.1557/jmr.2014.190.

[4] HAJNYS, J., PAGAC, M., KOTERA, O., PETRU, J., SCHOLZ, S. (2019). Influence of basic process parameters on mechanical and internal properties of 316L steel in SLM process for RENISHAW AM400. In: *MM Science Journal*. Vol. 2019, no. 01, pp. 2790-2794. ISSN 18031269. https://doi.org/10.17973/MMSJ.2019_03_2018127.

[5] HE, Y., ZHONG, M., BEUTH, J., WEBLER, B. (2020). A study of microstructure and cracking behavior of H13 tool steel produced by laser powder bed fusion using single-tracks, multi-track pads, and 3D cubes. In: *Journal of Materials Processing Technology*. Vol. 286. ISSN 09240136. https://doi.org/10.1016/j.jmatprotec.2020.116802.

[6] REN, B., LU, D., ZHOU, R., LI, Z., GUAN, J. (2019). Preparation and mechanical properties of selective laser melted H13 steel. In: *Journal of Materials Research*. Vol. 34, no. 08, pp. 1415-1425. ISSN 0884-2914. https://doi.org/10.1557/jmr.2019.10.

[7] MERTENS, R., VRANCKEN, B., HOLMSTOCK, N., KINDS, Y., KRUTH, J.-P., et al. (2016). Influence of Powder Bed Preheating on Microstructure and Mechanical Properties of H13 Tool Steel SLM Parts. In: *Physics Procedia*. Vol. 83, pp. 882-890. ISSN 18753892. https://doi.org/10.1016/j.phpro.2016.08.092.

[8] NARASIMHARAJU, S. R., ZENG, W., SEE, T. L., ZHU, Z., SCOTT, P., et al. (2022). A comprehensive review on laser powder bed fusion of steels: Processing, microstructure, defects and control methods, mechanical properties, current challenges and future trends. In: *Journal of Manufacturing Processes*. Vol. 75, pp. 375-414. ISSN 15266125. https://doi.org/10.1016/j.jmapro.2021.12.033.

[9] KOLOMY, S., SEDLAK, J., ZOUHAR, J., SLANY, M., BENC, M., et al. (2023). Influence of Aging Temperature on Mechanical Properties and Structure of M300 Maraging Steel Produced by Selective Laser Melting. In: *Materials*. Vol. 16, no. 3, p. 977. ISSN 1996-1944. https://doi.org/10.3390/ma16030977.

[10] YONEHARA, M., IKESHOJI, T., NAGAHAMA, T., MIZOGUCHI, T., TANO, M., et al. (2020). Parameter optimization of the high-power laser powder bed fusion process for H13 tool steel. In: T*he International Journal of Advanced Manufacturing Technology*. Vol. 110, no. 1-2, pp. 427-437. ISSN 0268-3768. https://doi.org/10.1007/s00170-020-05879-6.

[11] NARVAN, M., GHASEMI, A., FEREIDUNI, E., KENDRISH, S., ELBESTAWI, M. (2021). Part deflection and residual stresses in laser powder bed fusion of H13 tool steel. Vol. 204. ISSN 02641275. https://doi.org/10.1016/j.matdes.2021.109659.

[12] ABDEL-LATIF, M., ABDEL-GHANY, K., EL-MAHALLAWY, N., MATTAR, T. (2021). Effect of Laser Speed on Microstructure and Mechanical Properties of AISI H13 Tool Steel Prepared by Laser Powder Bed Fusion Process.

In: *Journal of Materials Engineering and Performance*. Vol. 30, no. 12, pp. 8821-8830. ISSN 1059-9495. https://doi.org/10.1007/s11665-021-06321-y.

[13] COOKE, S., AHMADI, K., WILLERTH, S., HERRING, R. (2020). Metal additive manufacturing: Technology, metallurgy and modelling. In: *Journal of Manufacturing Processes*. Vol. 57, pp. 978-1003. ISSN 15266125. https://doi.org/10.1016/j.jmapro.2020.07.025.

[14] OPELA, P., BENC M., KOLOMY, S., JAKUBEK, Z., BERANOVA D. (2023). High Cycle Fatigue Behaviour of 316L Stainless Steel Produced via Selective Laser Melting Method and Post Processed by Hot Rotary Swaging. In: *Materials*. Vol. 16, no. 9, p. 3400. ISSN 1996-1944. https://doi.org/10.3390/ma16093400.

[15] BOSE, A., REIDY, J. P., PÖTSCHKE, J. (2024). Sinter-based additive manufacturing of hardmetals: Review. In: *International Journal of Refractory Metals and Hard Materials*. Vol. 119. ISSN 02634368. https://doi.org/10.1016/j.ijrmhm.2023.106493.

[16] TIMKO, P., CZANOVA, T., CZAN, A., SLABEJOVA, S., HOLUBJAK, J., CEDZO, M. (2022). Analysis of Parameters of Sintered Metal Components Created by ADAM and SLM Technologies. In: *Manufacturing Technology* 2022, 22(3), 347-355 ISSN 12132489. doi:10.21062/mft.2022.032

[17] JANSA, J., VOLODARSKAJA, A., HLINKA, J., ZÁRYBNICKÁ, L., POLZER, S., et al. (2023). Corrosion and material properties of 316L stainless steel produced by material extrusion technology. In: *Journal of Manufacturing Processes*. Vol. 88, pp. 232-245. ISSN 15266125. https://doi.org/10.1016/j.jmapro.2023.01.035.

[18] CZAN, A., CZANOVA, T., HOLUBJAK, J., NOVAK, M., CZANOVA, N., CZAN, A., KRISAK, D. (2024). Analysis of the Basic Characteristics of the Working Accuracy of the Atomic Diffusion Additive Manufacturing ADAM Process by Comparison with the Selective Laser Melting SLM Process. In: *Manufacturing Technology*, **24**(1), 15-27 ISSN 12132489. doi:10.21062/mft.2024.015

[19] MAZUR, M., BRINCAT, P., LEARY, M., BRANDT, M. (2017). Numerical and experimental evaluation of a conformally cooled H13 steel injection mould manufactured with selective laser melting. In: *The International Journal of Advanced Manufacturing Technology*. Vol. 93, no. 1-4, pp. 881-900. ISSN 0268-3768. https://doi.org/10.1007/s00170-017-0426-7.

[20] LALEH, M., SADEGHI, E., REVILLA, R. I., CHAO, Q., HAGHDADI, N., et al. (2023). Heat treatment for metal additive manufacturing. In: *Progress in Materials Science*. Vol. 133. ISSN 00796425. https://doi.org/10.1016/j.pmatsci.2022.101051.

[21] KUMARAN, M., SENTHILKUMAR, V. (2023). Influence of Heat Treatment on Stainless Steel 316L Alloy Manufactured by Hybrid Additive Manufacturing Using Powder Bed Fusion and Directed Energy Deposition. In: *Metals and Materials International*. Vol. 29, no. 2, pp. 467-484. ISSN 1598-9623. https://doi.org/10.1007/s12540-022-01225-5.

[22] MCLEAN, N., BERMINGHAM, M.J., COLEGROVE, P., SALES, A., SORO, N., et al. (2022). Effect of Hot Isostatic Pressing and heat treatments on porosity of Wire Arc Additive Manufactured Al 2319. In: *Journal of Materials Processing Technology*. Vol. 310. ISSN 09240136. https://doi.org/10.1016/j.jmatprotec.2022.117769.

[23] GOHN, A. M., BROWN, D., MENDIS, G., FORSTER, S., RUDD, N., et al. (2022). Mold inserts for injection molding prototype applications fabricated via material extrusion additive manufacturing. In: *Additive Manufacturing*. Vol. 51. ISSN 22148604. https://doi.org/10.1016/j.addma.2022.102595.

[24] PAPAGEORGIOU, D., MEDREA, C., KYRIAKOU, N. (2013). Failure analysis of H13 working die used in plastic injection moulding. In: *Engineering Failure Analysis*. Vol. 35, pp. 355-359. ISSN 13506307. https://doi.org/10.1016/j.engfailanal.2013.02.028.

[25] KUO, C., XU, W. (2018). Effects of different cooling channels on the cooling efficiency in the wax injection molding process. In: *The International Journal of Advanced Manufacturing Technology*. Vol. 98, no. 1-4, pp. 887-895. ISSN 0268-3768. https://doi.org/10.1007/s00170-018-2345-7.

[26] HAJNYS, J., PAGAC, M., MESICEK, J., PETRU, J., SPALEK, F. (2020). Research of 316L Metallic Powder for Use in SLM 3D Printing. In: *Advances in Materials Science*. Vol. 20, no. 1, pp. 5-15. ISSN 2083-4799. https://doi.org/10.2478/adms-2020-0001.

[27] ISO 6892:2019 METALLIC MATERIALS. TENSILE TESTING. PART 1: METHOD OF TEST AT AMBIENT TEMPERATURE.

[28] SLOTWINSKI, J. A., GARBOCZI, E. J., HEBENSTREIT, K. M. (2014). Porosity Measurements and Analysis for Metal Additive Manufacturing Process Control. In: *Journal of Research of the National Institute of Standards and Technology*. Vol. 119. ISSN 2165-7254. https://doi.org/10.6028/jres.119.019.

[29] BECHNY, V., MATUS, M., JOCH, R., DRBUL, M., CZAN, A., SAJGALIK, M., NOVY, F. (2024) Influence of the Orientation of Parts Produced by Additive Manufacturing on Mechanical Properties. In: *Manufacturing Technology*, 24(1), 2-8. ISSN 12132489. doi:10.21062/mft.2024.021

[30] NOVAK, M., HAUSNEROVA, B., PATA, V., SANETRNIK, D. (2024). On the possibilities of merging additive manufacturing and powder injection molding in the production of metal parts. In: *Rapid Prototyping Journal*. Vol. 30, no. 11, pp. 50-58. ISSN 1355-2546. https://doi.org/10.1108/RPJ-02-2023-0047.

[31] ÅSBERG, M., FREDRIKSSON, G., HATAMI, S., FREDRIKSSON, W., KRAKHMALEV, P. (2019). Influence of post treatment on microstructure, porosity and mechanical properties of additive manufactured H13 tool steel. In: *Materials Science and Engineering: A*. Vol. 742, pp. 584-589. ISSN 09215093. https://doi.org/10.1016/j.msea.2018.08.046.

[32] FRYZOWICZ, K., DZIURKA, R., BARDO, R., MARCISZKO-WIąCKOWSKA, M., BAlA, P. (2023). Point-by-point laser exposure for crack susceptibility reduction in Powder Bed Fusion processing of H11 tool steel. In: *Journal of Materials Processing Technology*. Vol. 316. ISSN 09240136. https://doi.org/10.1016/j.jmatprotec.2023.117946.

[33] LIU, N., ZHENG, C., XIANG, D., HUANG, H., WANG, J. (2019). Effect of cutting parameters on tool wear under minimum quantity cooling lubrication (MQCL) conditions. In: *International journal of advanced manufacturing technology*. Vol. 105, no. 1-4, pp. 515-529. ISSN 0268-3768. https://doi.org/10.1007/s00170-019-04259-z.

[34] SARIKAYA, M., YILMAZ, V., GULLU, A. (2016). Analysis of cutting parameters and cooling/lubrication methods for sustainable machining in turning of Haynes 25 superalloy. In: *Journal of cleaner production*. Vol. 133, pp. 172-181. ISSN 0959-6526. https://doi.org/10.1016/j.jclepro.2016.05.122.

[35] OKONKWO, U., OKOKPUJIE, I., SINEBE, J., EZUGWU, Ch. (2015). Comparative analysis of aluminium surface roughness in end-milling under dry and minimum quantity lubrication (MQL) conditions. In: *Manufacturing review (Ulis, France)*. Vol. 2, p. 30. ISSN 2265-4224. https://doi.org/10.1051/mfreview/2015033.

[36] SYAHRI, B., PRASETYA, F., REFDINAL, R., SYAHRIAL, S. (2021). Effect of cutting speed on milling process on surface roughness of ST-37 steel material workpiece. In: *Jurnal Inovasi Vokasional dan Teknologi*. Vol. 21, no. 1, pp. 19-26. ISSN 1411-3414. https://doi.org/10.24036/invotek.v21i1.766.

[37] KOLOMY, S., MALY, M., SEDLAK, J., ZOUHAR, J., SLANY, M., et al. (2024). Machinability of extruded H13 tool steel: Effect of cutting parameters on cutting forces, surface roughness, microstructure, and residual stresses. In: *Alexandria Engineering Journal*. Vol. 99, pp. 394-407. ISSN 11100168. https://doi.org/10.1016/j.aej.2024.05.018.